Rotational excitation in D2–CO collisions

J. Andres, U. Buck, H. Meyer, and J. M. Launay

Citation: The Journal of Chemical Physics **76**, 1417 (1982); doi: 10.1063/1.443151
View online: http://dx.doi.org/10.1063/1.443151
View Table of Contents: http://scitation.aip.org/content/aip/journal/jcp/76/3?ver=pdfcov
Published by the AIP Publishing

Rotational excitation in D_2–CO collisions

J. Andres, U. Buck, and H. Meyer

Max-Plack-Institut für Strömungsforschung, D3400 Göttingen, Federal Republic of Germany

J. M. Launay

DAPHE, Observatoire de Meudon, 92190 Meudon, France
(Received 27 August 1981; accepted 28 September 1981)

In a crossed molecular beam experiment total differential cross sections and time of flight distibutions of the scattered particles have been measured for D_2 + CO at 87.2 meV collision energy. The energy loss spectra, which do not exhibit single rotational transitions, were transformed to the c.m. system so that not only positions but also amplitudes could be compared with calculations. The comparison shows that the spectra are dominated by two rotational rainbow peaks, one at large final rotational states j' due to the CO excitation on the C side of the molecule and one with larger probability at small j' due to the excitation on the O side of CO. The positions and the amplitudes of the former peak have been reproduced by the calculation using the *ab initio* potential [D. R. Flower, J. M. Launay, E. Kochanski, and J. Prissette, Chem. Phys. **37** 355 (1979)]; however, the amplitudes of the latter peak are overestimated but can be corrected by a smaller slope of the anisotropy of the potential. The parameters of the fitted isotropic potential $\epsilon = 5.73$ meV and $R_m = 3.88$ Å were found to deviate from the prediction. The calculations have been performed by treating D_2 in the j_z conserving coupled states approximation and CO in the infinite order sudden approximation.

I. INTRODUCTION

Rotational excitation is a fundamental process in gas phase collisions. It not only determines the very important transfer of rotational energy,[1] but since it is caused by the nonspherical part of the interaction potential, it also serves as an elegant tool for probing anisotropic molecular interactions.[1–3] The latter is especially true for state-to-state differential cross sections which have recently become available for a growing number of systems from crossed molecular beam experiments. With time of flight analysis of the scattered particles, H_2 and its isotopes have been studied in collision with ions[4,5] and neutrals.[6,7] Very recently, transitions for other molecules in collisions with He have been resolved.[8] With laser techniques much higher resolution can be obtained. Again these experiments are restricted to certain molecules like LiH[9] and Na_2.[10,11] On the other hand, interesting structures in the differential cross section for rotational excitation without complete state resolution have been reported for Li^+ + CO (Ref. 12) and K + CO, N_2 (Ref. 13) collisions. This "rotational rainbow" structure,[14–18] which manifests itself by an intensity peak in the energy loss spectra at fixed scattering angles, is of special value in the determination of anisotropic potentials[13(a),15(b),15(c)] as is the classical rainbow structure for the determination of isotropic interactions.[19]

A large variety of systems, especially molecule–molecule, have not been investigated so far. Thus, we have extended our experimental time of flight studies to the simple molecular system D_2 + CO. This system is of special interest in astrophysics. The rotational excitation of CO by H_2 impact is suggested as a possible mechanism for the excitation of CO lines in interstellar clouds. For this reason a potential surface has been calculated.[20,21] Experimental information is available for the spherically symmetric part of the potential from molecular beam experiments on the total differential[22] and integral[23] cross sections. The nonspherical part has been tested—at least in the attractive region—by a laser induced rotational relaxation study.[24] The present experiment is considered to give independent and, as far as the anisotropy is concerned, complementary information on the potential surface since rotational excitation is a sensitive probe of the repulsive part of the interaction.

From the theoretical point of view, the calculation of the cross sections which are relevant to this experiment by pure close-coupling methods is out of reach now since about 600 channels are strongly coupled, while calculations are still restricted to about 100 channels. However, there has been a considerable amount of work in the last ten years in the development of decoupling approximations and in the establishment of their conditions of validity. These tools, which are now well documented, are[25] (1) the centrifugal decoupling (CS) or j_z-conserving approximation introduced by McGuire and Kouri,[26] which is adapted to short range potentials. Its physical justification relies mainly on the fact that the intermolecular axis does not rotate during the collision. (2) The fixed-nuclei approximation, formerly introduced in nuclear physics by Chase,[27] has been widely used in electron–molecule scattering theory.[28] Its justification relies on two criteria: (a) the energy transferred during the collision is small compared to the kinetic energy of the relative motion; (b) the molecule does not rotate appreciably during the collision. (3) The infinite-order sudden approximation (IOS), introduced by Tsien and Pack,[29] is a combination of the j_z-conserving and fixed-nuclei approximations. It leads to a complete decoupling of the scattering equations and reduces the solution of the Schrödinger equation to the calculation of phase shifts parametrized by the angle γ between the internuclear axis and the intermolecular axis. It has the advantage to give, through the stationary phase approximation, a clear understanding of the rotational excita-

 0021-9606/82/031417-13$02.10

tion process, the transferred angular momentum being given by $2\partial\eta/\partial\gamma$, and the classical deflection angle by $2\partial\eta/\partial J$, where η is the phase shift and J the total angular momentum of the system.

For the problem we are considering, only the repulsive part of the potential is important. In addition, the fixed-nuclei approximation is approximately valid for the CO molecule but not for the D_2 molecule because of its larger rotational spacing. Although the coupling for D_2 is weak, which means that the distorted wave approximation should be valid, we prefer here to use a combination of two decoupling approximations, i.e., we will treat CO in the IOS approximation and D_2 in the j_z-conserving approximation. This results in a set of coupled differential equations parametrized by J and γ, the number of channels being equal to the number of rotational states included in the D_2 molecule. The scattering amplitudes are derived by directly projecting p-helicity states on r-helicity states which are best suited for the centrifugal decoupling approximations.

In order to compare the experimental energy loss spectra with calculations of state-to-state rotational transitions a special procedure was developed which allows the transformation of the complete spectrum into the center of mass (c.m.) system without losing information on the positions and amplitudes of the spectra. The comparison with calculated cross sections based on the *ab initio* potential surface[20,21] clearly shows that the data, though not state to state, are still a sensitive probe, mainly because of the rotational rainbow structure which survives in spite of possible double excitations and the more complicated molecule–molecule interaction.

The experiments—apparatus, results, and data evaluation—are described in Sec. II. The theoretical treatment is given in Sec. III. The comparison of experimental and theoretical data is made in Sec. IV. A discussion of the final results follows in Sec. V.

II. EXPERIMENTS

A. Apparatus

The details of the apparatus used in this work have been published elsewhere.[6(b),30] Briefly, the D_2 and the CO beams are produced as nozzle beams from two differentially pumped chambers and crossed at 90°. The scattered D_2 particles are detected by a double differentially pumped quadrupole mass spectrometer operating at pressures lower than 10^{-10} mbar. The angular dependence of the scattered beam intensity is measured by rotating the source assembly versus the fixed detector unit in the plane of the two intersecting beams. Elastic and inelastic events are separated by time of flight analysis of the scattered particles using the pseudorandom chopping technique. The D_2 gas was fed into a converter cryostat to produce o-D_2, which contains only even rotational states. The actual operating conditions of the beams are given in Table I. The large pumping facilities could only be used for the D_2 beam, since for CO the nozzle pressure had to be kept at relatively small values in order to avoid condensation.

TABLE I. Beam data.

	o-D_2	CO
Peak velocity (m/s)	2042	780
Nozzle diameter (μm)	10	100
Source pressure (bar)	191	6
Source temperature (K)	300	303
Speed ratio S	30.5	16.8
Angular divergence (deg)	1.7	4.0
Fraction in $j=0$	0.88	0.51
$j=1$	•••	0.43
$j=2$	0.12	0.06

A very important parameter for the interpretation of the data is the initial level population of the two beams. For the o-D_2 beam the problem has been discussed in detail in Refs. 30 and 31. Since the operating conditions are the same in the present case, we use the values obtained there. For CO, an infrared laser study on the relaxation of a CO beam has been published very recently.[32] For their best operating conditions (5 bar stagnation pressure p_0 and 40 μ nozzle diameter D) the level population is 0.34 for $j=0$, 0.42 for $j=1$, 0.18 for $j=2$, and 0.06 for $j=3$. The distribution cannot be described by a temperature. The rotational energy based on this result is $E_{rot}=0.63$ meV. A careful energy balance where real gas effects have been accounted for[33] gives for the operating conditions of Ref. 32 ($p_0 \cdot D = 200$ bar μm) and the present experimental arrangement $E_{rot}=0.43\pm0.25$ and 0 ± 0.25 meV, respectively. This result, which is in agreement with the findings of Ref. 32, though of much less accuracy, clearly indicates that a better expansion gives an enhancement of the lower rotational states. This conclusion is supported by a small amount of de-excitation found in an experiment on He + CO,[8] where single transitions have nearly been resolved. The analysis and comparison of the $1\rightarrow0$ and $0\rightarrow1$ transitions give 0.55 for $j=0$ and 0.41 for $j=1$ under the operating condition of the nozzle source of $p_0 \cdot D = 800$ bar μm. Since our operating values (6 bar at 100 μm) are between the two direct measurements, the values of Table I have been interpolated between the two results.

B. Experimental results

The experimental results obtained in the laboratory at the energy of $E=87.2$ meV, which corresponds to the data of Table I, are displayed in Figs. 1 and 2. Figure 1 shows the total differential cross sections, i.e., the sum over all elastic and inelastic channels. The attractive well of the system is so small compared to the collision energy that no rainbow structure shows up. The remaining diffraction oscillations are clearly resolved though they appear to be somewhat damped compared to a purely elastic case.[34,35] Figure 2 shows the measured time of flight spectra at six different laboratory angles. The spectra are normalized to their maximum intensities. Clearly, the resolution is not sufficient to re-

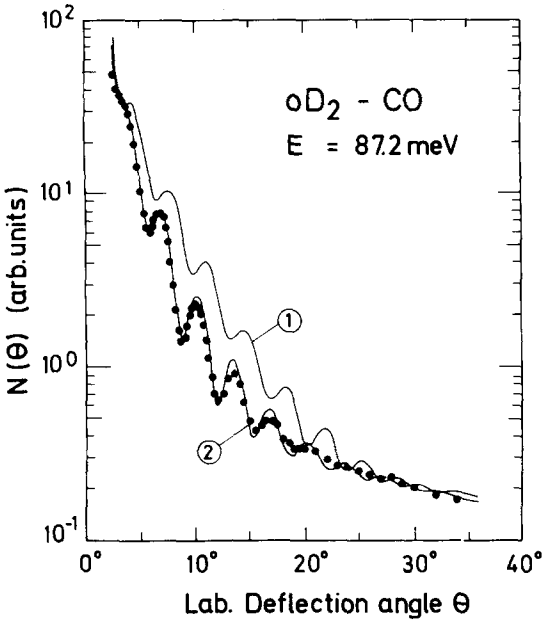

FIG. 1. Measured and calculated total differential cross sections. Curve (1): calculation using the *ab initio* potential of Ref. 21. Curve (2): calculation using the fitted isotropic potential of Sec. IV A and the anisotropy of Ref. 21.

solve single transitions. However, some features are remarkable. The steep rise of the spectra at negative time differences indicates that almost no de-excitations take place, in agreement with the conclusion of the last section that both molecules are in their lowest possible states. The maximum intensity is shifted slightly towards larger flight times and at large angles a shoulder appears, which increases with increasing scattering angle.

C. Data analysis and averaging processes

For the comparison of the measured data to calculations the different averaging processes of the apparatus and the beam properties have to be carefully taken into account. The present analysis is based on the procedure described in detail in Ref. 30, which gives, for the scattered beam number density (particles per cm^3) at a given laboratory (lab) angle θ and a final velocity v_f for the transition i to f

$$N_{if}(\theta, v_f) = n_1 n_2 \, \Delta V \, \Delta\Omega(\theta) p_i \int dv_f' D(v_f, v_f') v_f'^{-1} \times \int dg d\vartheta \, \sigma_{if}(g, \vartheta) F_{if}(g, \vartheta, v_f') \,, \quad (1)$$

where ϑ is the deflection angle in the center-of-mass (c.m.) system, n_1 and n_2 are the averaged densities of the two beams in the scattering volume ΔV, p_i is the relative population of the state i, and g is the relative velocity. The factor $\Delta V \Delta\Omega(\theta)$ accounts for the finite dimensions of the scattering center and the detector and $v_F'^{-1}$ for the velocity dependence of the detection system. $D(v_f, v_f')$ is a dimensionless transmission function of the velocity analyzer, which also accounts for the finite ionization volume. The key point is the distribution function $F_{if}(g, \vartheta, v_f')$ which is calculated by a Monte Carlo simulation over the velocity *and* angular distributions of the two intersecting beams. It contains, in addition, the relative velocity g and the Jacobian for the transformation from the c.m. to the lab system $J = v_f^2 / u_f^2 \cos(u_f, v_f)$, where u_f denotes the final c.m. velocity. Note that the indices $i = (j_1, j_2)$ and $f = (j_1', j_2')$ mark two states, one for each molecule, while 1 and 2 indicates the molecules D_2 and CO, respectively.

For the analysis of the total differential cross sections the dependence on v_f is not measured and the expression is appreciably simplified. The resulting distribution function can be well approximated by a product of a Guassian in g and a rectangular distribution in ϑ with the full width at half-maximum (FWHM) of $\Delta g/g = 0.05$ and a full width of $\Delta\vartheta_0 = 0.99°$.

For the time of flight distribution we have to start from Eq. (1). Since single rotational transitions have not been resolved, the measured time of flight spectra cannot be transformed in an unambiguous way to state-to-state cross sections in the c.m. system, as has been described in detail in Ref. 30. An additional complication arises from the fact that both the D_2 and the CO molecule can be excited with the same energy loss, which cannot be distinguished by the present experimental method. One possible solution to this problem is a straightforward application of Eq. (1) with the calculated cross section σ_{if} as input information. We have to sum up all cross sections which correspond to energy losses

$$\Delta E_{if} = B_2[j_2'(j_2'+1) - j_2(j_2+1)] + B_1[j_1'(j_1'+1) - j_1(j_1+1)] \,. \quad (2)$$

Such a procedure has to be repeated for all initial states in the two beams. However, with help of the factorization formula for the cross sections [see Eq. (37)] this procedure can be reduced to the σ_{0f} values. After performing all averaging, the calculated intensity value for

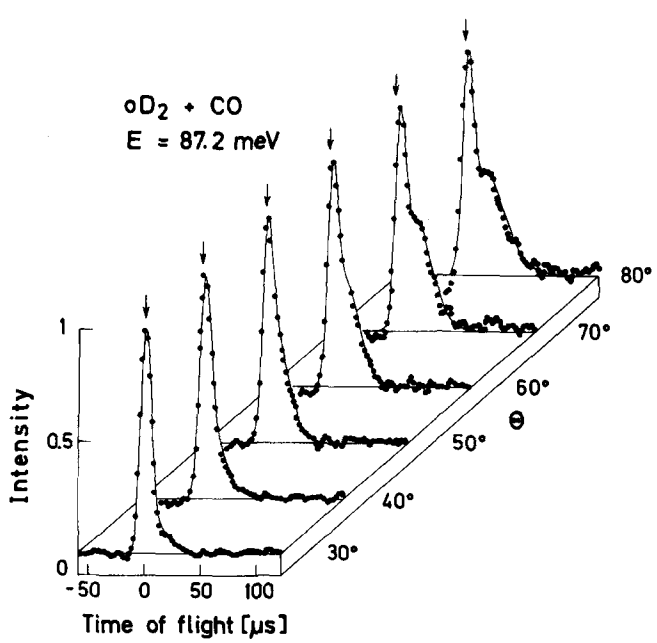

FIG. 2. Measured time of flight spectra at different laboratory deflection angles. The spectra are normalized to the maximum. The arrows indicate the position of the elastic transition.

every ΔE_{if} can be compared with the measured points in the lab system. Such a procedure, though it is unambiguous, has the disadvantage that for every comparison the whole calculation has to be repeated. In addition, lab distributions give no (or at least only reduced) physical insight into the origin of the measured phenomena. Thus, it seems worthwhile to employ the other method which is the transformation of the data to the c.m. system where any comparison with theory is much more feasible. However, such a comparison requires that the transformation not only contains information on the nominal c.m. velocities[13] but also on the amplitudes of the distribution functions.

To solve this problem we first of all proceed as described in Ref. 30. Under the assumption that the cross section and the Jacobian vary only slowly in the narrow range of the distribution functions, the integration over g and ϑ can be carried out over the distribution functions of the two beams and the result is convoluted with the function D, which contains contributions from the finite ionization range (12 mm from 446 mm flight path), the shutter function of the chopper (4 μs), and the channel width of the time of flight analyzer (2 μs). The FWHM of the resulting distribution functions G_{if} does not vary for different transitions and only slightly changes over the measured angular range. The remaining amplitude of G_{if} is directly related to the cross sections by

$$A_{if} = K p_i \bar{J}_{if} \sigma_{if}(\bar{\vartheta}, \bar{g}) \ , \tag{3}$$

where K only contains variables which depend on θ and $\sigma_{if}(\bar{\vartheta}, \bar{g})$ is the most probable value of the cross section. Now the measured spectra are fitted to the calculated functions G_{if} according to

$$N(\theta, v_f) = \sum_{if} A_{if} G_{if}(\theta, v_f) v_f^{-1} \ , \tag{4}$$

where the summation is over the different initial states and also accounts for the fact that different i/f values lead to the same ΔE_{if} or v_f. The resulting cross sections are not expected to give the correct answer. Since the half-width of G_{if} in the v_f space of 116 to 150 m/s is always larger than the difference for single rotational transitions of CO which varies from a few m/s to 100 m/s, a fitting procedure for so many states with the additional ambiguity of a simultaneous D_2 and CO excitation will not lead to a unique solution.

However, if we average this result over the experimental distribution function in the energy space, we should get a reliable answer. In order to derive the correct distribution function, we go back to Eq. (1), replace the cross sections by their most probable values [as in Eq. (3)], perform the integration over dv_f and $d\vartheta$, and transform the result from g to E space. The result is

$$I(\vartheta, \Delta E) = K \sum_{if} p_i \sigma_{if}(\bar{\vartheta}, \bar{g}) H_{if}(\Delta E) \ , \tag{5}$$

with $H_{if} = (\sqrt{\pi} \cdot B)^{-1} \exp[-(\Delta E_{if} + \Delta E)^2 / B^2]$ and $\Delta E = E - E_0$. For the present experiment we have $E_0 = 87.2$ meV and $B = 5.44$ meV, which correspond to 9.05 meV FWHM. Equation (5) represents a summation over Gaussian distribution functions centered at ΔE_{if} whose area is

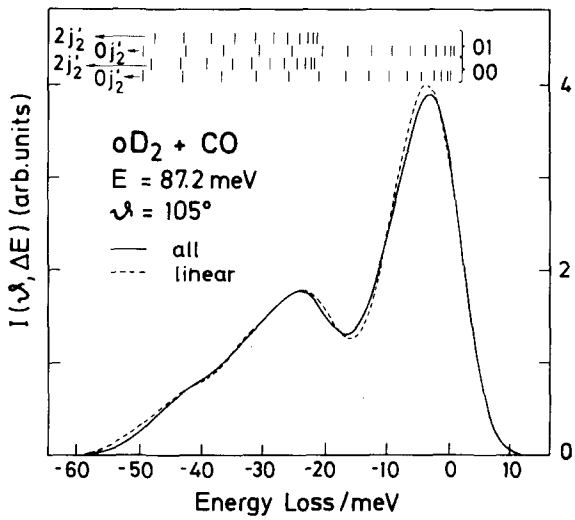

FIG. 3. Measured time of flight spectra transformed into the c.m. system using the method of Sec. IIC. The solid line is the result when all possible transitions indicated in the upper part are used as grid points. The dashed line is derived from equally spaced grid points for the transferred energy. The index 1 stands for D_2 and index 2 for CO.

equal to the cross section. These intensity values should be very reliable for any comparison with theory provided that the theoretical calculations are subject to the same averaging procedure. This procedure is, contrary to the full averaging according to Eq. (1), easy to perform and arises sometimes, e.g., for classical trajectory calculations, in a very natural way.

Figure 3 shows the intensity distributions $I(\vartheta, \Delta E)$ developed in this way for two different sets of ΔE values: the ones given by Eq. (2) and listed in the upper part of the figure, and, because of the high density of states, equally spaced values. Since three initial states of CO are populated, which are correlated by using the factorization relation Eq. (37), a lot of possible states are open. Note the opening of a new series of channels for the $0 \rightarrow 2$ excitation of D_2. The results are nearly identical for the two different choices of ΔE values (which is not the case for the unaveraged values).[35] Thus, we conclude that this procedure indeed represents a reliable method of transforming unresolved spectra to the c.m. system. It should be noted that in the present case the c.m. angle only varies from 104.9° for the elastic transition to 107° for the largest ΔE values measured. Thus, it proved not to be necessary to interpolate the measured values in order to arrive at a fixed c.m. angle. Generally, a weighted averaged value is given.

The final experimental results are displayed in Fig. 4 for all available data. Now it is much easier to discuss the physical content of the measurement than it would have been in the lab system: (i) The spectra are dominated by a maximum at small values of the transferred energy which corresponds to small values of the final rotational state of CO j_2'. (ii) This maximum is slightly shifted to larger values of ΔE or j_2' with increasing scattering angle. (iii) At larger ΔE (and j_2') values a second maximum appears which increases by a larger amount than the first maximum with increasing scat-

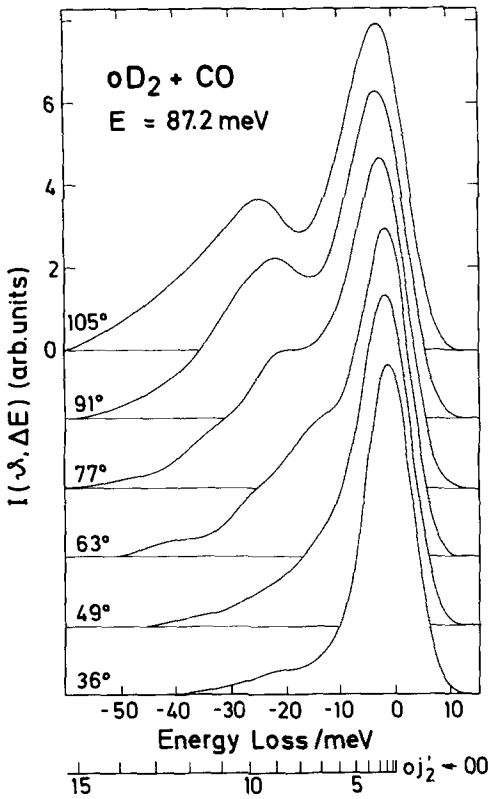

FIG. 4. Measured time of flight spectra in the c.m. system for all angles measured. The scale in the lower part shows possible pure CO transitions.

tering angle. (iv) The amount of transferred energy reaches 6 and 25 meV in the two peaks and goes to zero at about 55 meV at the largest scattering angle corresponding to a $\Delta j = 15$ transition of CO.

We would like to point out that the curves presented in Figs. 3 and 4 do not contain any deconvolution procedure. Thus, the second maxima which appear in these spectra are only due to the Jacobian of the lab–c.m. transformation. However, the concentration of all average effects into a single function would simplify a deconvolution appreciably. Any standard procedure available in the literature can be used for such a deconvolution.[36]

The present procedure to evaluate the data is very similar to the method published by Shimamura[37] which was brought to our notice after the completion of the present work. Contrary to his conclusion, we do not believe that we are able to extract state-to-state cross sections from this type of measurement. However, the conditions of our experiment and Shimamura'a are complementary. Whereas we have to deal with three initial states and a large number of final states, the experimental situation of Ref. 37 is the other way round, which favors an unambiguous evaluation.

III. THEORY

A. Background

The determination of differential cross sections from the potential energy surface calculated in Refs. 20 and 21 cannot be presently performed without approximations because of the large number of strongly coupled channels as mentioned in the Introduction.

The implementation of the now widely used centrifugal decoupling approximation, introduced by McGuire and Kouri and Pack[26] in atom–diatom collisions, permits the drastic reduction of the number of coupled equations to solve but necessitates the formulation of the scattering equations in a body-fixed frame of reference, with a quantization axis lying along the intermolecular axis. A decoupling of the equations results from the neglect of rotational coupling, and a basis of states where the r helicity $\Omega = \mathbf{j} \cdot \hat{r}$ is a good quantum number is best suited for that purpose.[25,26,38]

On the other hand, it has been shown by Jacob and Wick[39] that differential cross sections could be expressed in a simple form when using a basis where the p helicity $\lambda = \mathbf{j} \cdot \hat{k}$ is a good quantum number. Applications of this formalism to molecular collisions have been developed by Klar.[40]

Since the IOS approximation involves also centrifugal decoupling, we have to use both bases and we will in a first step give the relation between the r-helicity and p-helicity bases for two diatomic molecules (Sec. III B), generalizing the work of Moses.[41] We shall then derive the scattering equations, treating one molecule in the IOS approximation, and the other in the centrifugal decoupling approximation (Sec. III C), derive scattering amplitudes (Sec. III D), and demonstrate generalized factorization relations between cross sections (Sec. III E). A brief discussion of results will follow (Sec. III F).

In the following, we shall use the conventions of Rose[42] and Messiah[43] for Euler angles, rotation matrices, and spherical harmonics.

B. r-helicity and p-helicity bases

We consider the collision of two $^1\Sigma$ diatomic molecules leading to rotational excitation. We first define plane wave states

$$|\mathbf{k} j_1 \lambda_1 j_2 \lambda_2\rangle = R(\varphi_k \theta_k - \varphi_k) \, |k\hat{z} j_1 \lambda_1 j_2 \lambda_2\rangle \ , \tag{6}$$

where j_1 and j_2 are the angular momenta of molecules 1 and 2, respectively, $\lambda = \mathbf{j} \cdot \hat{k}$ their p helicity, (θ_k, φ_k) the polar angles of the wave vector $\mathbf{k}$ and $\hat{z}$ a unit vector directed along the z axis. R is a rotation of angle φ_k around the unit vector $\hat{z} \times \hat{k}$, where $\hat{k} = \mathbf{k}/k$.

The plane wave states defined in Eq. (6) can be expanded over eigenfunctions of $|\mathbf{k}|$, $\mathbf{j}_1^2$, $\mathbf{j}_1 \cdot \hat{k}_1$, $\mathbf{j}_2^2$, $\mathbf{j}_2 \cdot \hat{k}_2$, $\mathbf{J}^2$, and J_z, where $\mathbf{J} = \mathbf{l} + \mathbf{j}_1 + \mathbf{j}_2$ is the total angular momentum (orbital l and internal $\mathbf{j}_1 + \mathbf{j}_2$) of the system, according to the expression

$$|\mathbf{k} j_1 \lambda_1 j_2 \lambda_2\rangle = \sum_{JM} \left(\frac{2J+1}{4\pi}\right)^{1/2} \times D^J_{M\lambda}(\varphi_k \theta_k - \varphi_k) \, |k j_1 \lambda_1 j_2 \lambda_2 JM\rangle \ , \tag{7}$$

where $\lambda = \lambda_1 - \lambda_2$ is the projection of $\mathbf{j}_1 + \mathbf{j}_2$ on $\hat{k}$. The minus sign in λ arises because helicities refer to the direction of motion of each particle, whereas $\hat{k}$ points in direction of motion of 1 relative to 2.

Equation (7) can be rewritten as

$$|kj_1\lambda_1 j_2\lambda_2 JM\rangle = \left(\frac{2J+1}{4\pi}\right)^{1/2} \int D^{J*}_{M\lambda}(\varphi_k\theta_k - \varphi_k) \times |\mathbf{k}j_1\lambda_1 j_2\lambda_2\rangle \sin\theta_k\, d\theta_k\, d\varphi_k \ . \quad (8)$$

We define analogously r-helicity states

$$|\mathbf{r}j_1\Omega_1 j_2\Omega_2\rangle = R(\varphi_r\theta_r - \varphi_r)|r\hat{z}j_1\Omega_1 j_2\Omega_2\rangle \ , \quad (9)$$

where $\mathbf{r} = \mathbf{r}_2 - \mathbf{r}_1$ is the intermolecular vector directed from molecule 2 to molecule 1.

We expand these states over eigenfunctions of $\mathbf{j}_1^2$, $\mathbf{j}_1\cdot\hat{r}_1$, $\mathbf{j}_2^2$, $\mathbf{j}_2\cdot\hat{r}_2$, $|\mathbf{r}|$, $\mathbf{J}^2$, and J_z:

$$|\mathbf{r}j_1\Omega_1 j_2\Omega_2\rangle = \sum_{JM}\left(\frac{2J+1}{4\pi}\right)^{1/2} D^J_{M\Omega}(\varphi_r\theta_r - \varphi_r) \times |rj_1\Omega_1 j_2\Omega_2 JM\rangle \ , \quad (10)$$

where $\Omega = \Omega_1 - \Omega_2$ is the projection of $\mathbf{j}_1 + \mathbf{j}_2$ on $\hat{r}$.

Equation (5) can also be rewritten as

$$|rj_1\Omega_1 j_2\Omega_2 JM\rangle = \left(\frac{2J+1}{4\pi}\right)^{1/2} \int D^{J*}_{M\Omega}(\varphi_r\theta_r - \varphi_r) \times |\mathbf{r}j_1\Omega_1 j_2\Omega_2\rangle \sin\theta_r\, d\theta_r\, d\varphi_r \ . \quad (11)$$

The relation between basis states defined by Eqs. (8) and (11) is given by their scalar product

$$\langle rj_1\Omega_1 j_2\Omega_2 JM|kj_1\lambda_1 j_2\lambda_2 JM\rangle = 4\pi\sum_{l j_{12}\lambda\Omega} i^l(2l+1)(2j_{12}+1)\begin{pmatrix} j_{12} & l & J\\ \lambda & 0 & -\lambda\end{pmatrix}\begin{pmatrix} j_{12} & l & J\\ \Omega & 0 & -\Omega\end{pmatrix}\begin{pmatrix} j_1 & j_2 & j_{12}\\ \Omega_1 & -\Omega_2 & -\Omega\end{pmatrix}\begin{pmatrix} j_1 & j_2 & j_{12}\\ \lambda_1 & -\lambda_2 & -\lambda\end{pmatrix} j_l(kr) \ . \quad (12)$$

Using the asymptotic form of spherical Bessel functions, we derive the large r behavior of the scalar product

$$\langle rj_1\Omega_1 j_2\Omega_2 JM|kj_1\lambda_1 j_2\lambda_2 JM\rangle \underset{r\to\infty}{\sim} \frac{2\pi}{ikr}\left[e^{+ikr}\delta_{\lambda_1\Omega_1}\delta_{\lambda_2\Omega_2} - (-)^{J+j_1+j_2}\delta_{\lambda_1-\Omega_1}\delta_{\lambda_2-\Omega_2}e^{-ikr}\right] \ , \quad (13)$$

which shows that, for the divergent wave, the r and p helicities are the same because the $\mathbf{r}_i$ are in the same direction as the $\mathbf{k}_i$, whereas for the convergent wave the situation is reversed. Using Eqs. (7) and (13), we can write the asymptotic decomposition of the plane wave

$$|\mathbf{k}j_1\lambda_1 j_2\lambda_2\rangle \underset{r\to\infty}{\sim} \sum_{JM\Omega_1\Omega_2}\frac{1}{kr}(2J+1)\pi\ i^{J+j_1+j_2+1}D^J_{M\lambda}(\varphi_k\theta_k - \varphi_k)\left(\delta_{\lambda_1-\Omega_1}\delta_{\lambda_2-\Omega_2}\exp\{-i[kr-(J+j_1+j_2)(\pi/2)]\}\right.$$
$$\left. - \delta_{\lambda_1\Omega_1}\delta_{\lambda_2\Omega_2}\exp\{i[kr-(J+j_1+j_2)(\pi/2)]\}\right)|rj_1\Omega_1 j_2\Omega_2 JM\rangle \ . \quad (14)$$

This equation will be useful later to relate S-matrix elements in the r-helicity basis to S-matrix elements in the p-helicity basis.

C. Scattering equations

The Hamiltonian for the system of two interacting diatomic molecules can be written as

$$H = \left(-\frac{1}{2\mu r}\frac{\partial^2}{\partial r^2}r + \frac{\mathbf{l}^2}{2\mu r^2} + B_1\mathbf{j}_1^2 + B_2\mathbf{j}_2^2 + V\right) \ , \quad (15)$$

where μ is the reduced mass of the system, B_1 and B_2 the rotational constants of each molecule, and V the interaction potential. In the following, we will consider that molecule 1 is D_2 while 2 is the CO molecule.

Expanding the wave function $|\psi\rangle$ of the system over the r-helicity states [Eq. (11)], we get coupled equations of a form similar to the ones derived by Klar[40] and Launay.[44] We approximate these equations first by replacing $\mathbf{l}^2$ by $\mathbf{J}^2$, which is consistent with the centrifugal decoupling approximation in the atom–diatom case,[25,26,38] and second by putting $B_2 = 0$, which is consistent with the IOS approximation for the heavy CO molecule.[25,26] The justification of the centrifugal decoupling approximation relies on the fact that, for short ranged potentials, little rotation of the intermolecular axis occurs during the collisions; the justification of the second approximation relies on the fact that the CO molecule does not rotate during the collision.

The approximate Hamiltonian can now be written as

$$\tilde{H} = -\frac{1}{2\mu r}\frac{\partial^2}{\partial r^2}r + \frac{\mathbf{J}^2}{2\mu r^2} + B_1\mathbf{j}_1^2 + V \ . \quad (16)$$

To solve the Schrödinger equation corresponding to the Hamiltonian (16), we consider a basis of states where the angle γ_2 between molecule 2 and $\hat{r}$ is fixed:

$$|rj_1\Omega_1\gamma_2\Omega_2 JM\rangle = \left(\frac{2J+1}{4\pi}\right)^{1/2}\int D^{J*}_{M\Omega}(\varphi_r\theta_r - \varphi_r) \times |\mathbf{r}j_1\Omega_1\gamma_2\Omega_2\rangle \sin\theta_r\, d\theta_r\, d\varphi_r \ , \quad (17)$$

where

$$|\mathbf{r}j_1\Omega_1\gamma_2\Omega_2\rangle = R(\varphi_r\theta_r - \varphi_r)|r\hat{z}j_1\Omega_1\gamma_2\Omega_2\rangle \quad (18)$$

and

$$\langle\theta_1\varphi_1\theta_2\varphi_2|\, j_1\Omega_1\gamma_2\Omega_2\rangle = Y_{j_1\Omega_1}(\theta_1\varphi_1)\, e^{i\Omega_2\varphi_2}\delta(\theta_2 - \gamma_2)(\sin\theta_2)^{-1} \ . \quad (19)$$

This basis is continuous in the angle γ_2 and does not diagonalize any more $\mathbf{j}_2^2$. The relations between bases (17) and (11) can be written as

$$|rj_1\Omega_1\gamma_2\Omega_2 JM\rangle = \sum_{j_2}\frac{P_{j_2\Omega_2}(\gamma_2)}{\sqrt{2\pi}}|rj_1\Omega_1 j_2\Omega_2 JM\rangle \ , \quad (20)$$

when the $P_{j_2\Omega_2}(\gamma_2)$ are associated Legendre polynomials.

The orbital and rotational kinetic energy terms $\mathbf{J}^2/2\mu r^2$ and $B_1\mathbf{j}_1^2$, respectively, in $\tilde{H}$ are diagonal in

this basis; however, the interaction potential, which conserves the projection $\Omega_1 - \Omega_2$ of $\mathbf{j}_1 + \mathbf{j}_2$ on $\hat{r}$ but not Ω_1 and Ω_2 separately, has nondiagonal elements due to torsion effects.

We recall here the expression of the *ab initio* potential calculated in Refs. 20 and 21

$$V = \sum_{q_1 q_2 \mu} V_{q_1 q_2 \mu}(r)\, Y_{q_1 q_2 \mu}(\hat{R}_1 \hat{R}_2) \ , \tag{21}$$

where

$$Y_{q_1 q_2 \mu}(\hat{R}_1 \hat{R}_2) = 4\pi \left[2(1+\delta_{\mu 0})\right]^{-1/2} \times \left[Y_{q_1 \mu}(\hat{R}_1)\, Y_{q_2 -\mu}(\hat{R}_2) + Y_{q_1 -\mu}(\hat{R}_1)\, Y_{q_2 \mu}(\hat{R}_2)\right] . \tag{22}$$

Torsion effects in the expansion (21) are due to terms with nonvanishing μ. At short distances, where rotational excitation is important, they are much smaller than the other terms ($v_{222}/v_{200} \simeq 0.1$, $v_{222}/v_{020} \simeq 0.01$ for $r = 5a_0$). We neglect these terms with $\mu \neq 0$ and the potential which is now diagonal in the basis (17) can be expressed as

$$\tilde{V} = \sum_{q_1 q_2} (2q_1+1)^{1/2} (2q_2+1)^{1/2} v_{q_1 q_2 0}(r)\, P_{q_1}(\cos\gamma_1)\, P_{q_2}(\cos\gamma_2) \ , \tag{23}$$

where P_{q_1} and P_{q_2} are the usual Legendre polynomials.

The expansion of the wave function in basis (17) can be written now as

$$|\Psi\rangle = \sum_{\Omega_2 j_1 \Omega_1} \int \sin\gamma_2 d\gamma_2 \frac{1}{r} F^{J;\Omega_1\gamma_2\Omega_2}_{j_1}(r) \left| j_1 \Omega_1 \gamma_2 \Omega_2 JM \right\rangle \tag{24}$$

and the corresponding coupled equations

$$\left[\frac{d^2}{dr^2} - \frac{J(J+1)}{r^2} + k^2_{j_1}\right] F^{J;\Omega_1\gamma_2\Omega_2}_{j_1}(r) = 2\mu \sum_{j'_1} \tilde{V}^{\Omega_1\Omega_2}_{j_1 j'_1}(r;\gamma_2)\, F^{J;\Omega_1\gamma_2\Omega_2}_{j'_1}(r) \ , \tag{25}$$

where

$$\tilde{V}^{\Omega_1\Omega_2}_{j_1 j'_1}(r;\gamma_2) = \sum_{q_2} (-)^{\Omega_1} (2q_1+1)^{1/2} (2q_2+1)^{1/2} (2j_1+1)^{1/2} (2j'_1+1)^{1/2} \times \begin{pmatrix} j_1 & q_1 & j'_1 \\ 0 & 0 & 0 \end{pmatrix} \begin{pmatrix} j_1 & q_1 & j'_1 \\ \Omega_1 & 0 & -\Omega_1 \end{pmatrix} P_{q_2}(\cos\gamma_2)\, v_{q_1 q_2 0}(r) \tag{26}$$

and $k^2_{j_1} = 2\mu[E - B_1 j_1(j_1+1)]$.

D. Derivation of scattering amplitudes and differential cross section

The boundary conditions for Eq. (25) are

$$F^{J;\Omega_1\gamma_2\Omega_2}_{j'_1 j_1}(r) \underset{r\to\infty}{\sim} \frac{1}{k^{1/2}_{j_1}} \exp\{-i[k_{j_1} r - (J\pi/2)]\}\, \delta_{j'_1 j_1} - \frac{1}{k^{1/2}_{j'_1}} \exp\{i[k_{j'_1} r - (J\pi/2)]\}\, S^{J;\Omega_1\gamma_2\Omega_2}_{j'_1 j_1} \ . \tag{27}$$

Relation (20) permits the introduction of the rotational angular momentum j_2 in S-matrix elements

$$S^{J;\Omega_1\Omega_2}_{j'_1 j'_2 j_1 j_2} = \int_0^\pi S^{J;\Omega_1\gamma_2\Omega_2}_{j'_1 j_1} P_{j_2\Omega_2}(\gamma_2)\, P_{j'_2\Omega_2}(\gamma_2) \sin\gamma_2 d\gamma_2 \ . \tag{28}$$

Scattering amplitudes in the p-helicity representation are given by the usual formula[39]

$$f_{j'_1\lambda'_1 j'_2\lambda'_2; j_1\lambda_1 j_2\lambda_2}(\mathbf{k}_f \mathbf{k}_i) = \frac{i}{2(k_i k_f)^{1/2}} \sum_{JM} (2J+1) \times T^J_{j'_1\lambda'_1 j'_2\lambda'_2; j_1\lambda_1 j_2\lambda_2} D^{J*}_{M\lambda'}(\varphi_f \theta_f - \varphi_f)\, D^J_{M\lambda}(\varphi_i \theta_i - \varphi_i) \ , \tag{29}$$

where $\mathbf{k}_i$ and $\mathbf{k}_f$ refer to the initial and final momentum values, respectively. The plane wave decomposition (14), the centrifugal decoupling approximation which involves conservation of Ω, and Relation (13) give the expression of the p-helicity S-matrix elements as a function of the approximate S in Eq. (28):

$$S^J_{j'_1\lambda'_1 j'_2\lambda'_2; j_1\lambda_1 j_2\lambda_2} = i^{j_1+j_2+j'_1+j'_2}\, S^{J;-\lambda_1-\lambda_2}_{j_1 j_2 j'_1 j'_2}\, \delta_{\lambda'_1-\lambda_1}\, \delta_{\lambda'_2-\lambda_2} \ . \tag{30}$$

Using Eqs. (28) and (30), we can compute the scattering amplitudes (29) in two steps; first we calculate fixed angle scattering amplitudes in the r-helicity basis

$$f^{\Omega_1\Omega_2}_{j'_1 j_1}(\mathbf{k}_f \mathbf{k}_i; \gamma_2) = \frac{i}{2(k_i k_f)^{1/2}} \sum_{JM} (2J+1)\, T^{J;\Omega_1\gamma_2\Omega_2}_{j'_1 j_1} \times D^{J*}_{M-\Omega}(\varphi_f \theta_f - \varphi_f)\, D^J_{M\Omega}(\varphi_i \theta_i - \varphi_i) \ . \tag{31}$$

We then obtain Eq. (29) by a simple quadrature over γ_2:

$$f_{j'_1\lambda'_1 j'_2\lambda'_2; j_1\lambda_1 j_2\lambda_2}(\mathbf{k}_f \mathbf{k}_i) = i^{j_1+j_2+j'_1+j'_2}\, \delta_{\lambda'_1-\lambda_1}\, \delta_{\lambda'_2-\lambda_2} \times \int_{f_{j'_1 j_1}}^{-\lambda_1-\lambda_2} (\mathbf{k}_f \mathbf{k}_i; \gamma_2) \sin\gamma_2 d\gamma_2 \ . \tag{32}$$

Differential cross sections are finally computed by the usual formula

$$\left.\frac{d\sigma}{d\Omega}\right|_{j'_1 j'_2; j_1 j_2} = \frac{1}{(2j_1+1)(2j_2+1)} \frac{k_f}{k_i} \times \sum_{\lambda_1\lambda_2\lambda'_1\lambda'_2} \left| f_{j'_1\lambda'_1 j'_2\lambda'_2; j_1\lambda_1 j_2\lambda_2}(\mathbf{k}_f \mathbf{k}_i) \right|^2 \ . \tag{33}$$

We see in Eqs. (30)–(32) that the approximate IOS S-matrices and scattering amplitudes involve a flip in the p helicity λ. This is an effect of the centrifugal decoupling approximation which implies the conservation of the r helicity Ω.

E. Factorization relations between differential cross sections

We will generalize here the factorization relations demonstrated for the atom–diatom case in the framework of the IOS and CS approximations.[45] Such a generalization has already been performed for diatom–diatom relaxation cross sections[46] when one diatomic can be considered as fixed in space during the collision.

We start from the Born–Oppenheimer approximation for scattering states[27] which results in a factorization of scattering amplitudes

$$f_{j'_1 m'_1 j'_2 m'_2; j_1 m_1 j_2 m_2}(\mathbf{k}_f \mathbf{k}_i) = \int Y^*_{j'_2 m'_2}(\hat{R}_2) \times f_{j'_1 m'_1 j_1 m_1}(k_f k_i; \hat{R}_2)\, Y_{j_2 m_2}(\hat{R}_2)\, d\hat{R}_2 \ , \tag{34}$$

in which the m quantum numbers are spaced fixed projections and the scattering amplitude on the right-hand side refers to the collision of molecule 1 on molecule 2 in the fixed position $\hat{R}_2$. Using the composition theorem

of spherical harmonics, we obtain

$$f_{j_1'm_1'j_2'm_2';j_1m_1j_2m_2}(\mathbf{k}_f\mathbf{k}_i) = (-)^{m_2}\sum_{\kappa m_\kappa}[(2j_2+1)(2j_2'+1)(2\kappa+1)]^{1/2} \times\begin{pmatrix} j_2 & j_2' & \kappa \\ 0 & 0 & 0\end{pmatrix}\begin{pmatrix} j_2 & j_2' & \kappa \\ m_2 & -m_2' & m_\kappa\end{pmatrix} f_{j_1'm_1'\kappa m_\kappa;j_1m_100}(\mathbf{k}_f\mathbf{k}_i) \quad (35)$$

From Eq. (35), we derive the relation

$$\left.\frac{d\sigma}{d\Omega}\right|_{j_1'j_2';j_1j_2} = \frac{k_f}{k_i}\frac{1}{(2j_1+1)}\sum_{\kappa m_\kappa m_1m_1'}(2j_2'+1) \times\begin{pmatrix} j_2 & j_2' & \kappa \\ 0 & 0 & 0\end{pmatrix}^2 |f_{j_1'm_1'\kappa m_\kappa;j_1m_100}(\mathbf{k}_f\mathbf{k}_i)|^2 \quad (36)$$

and, inserting the expression of differential cross sections with an initial $j_2=0$,

$$\left.\frac{d\sigma}{d\Omega}\right|_{j_1'j_2';j_1j_2} = \sum_\kappa(2j_2'+1)\begin{pmatrix} j_2 & j_2' & \kappa \\ 0 & 0 & 0\end{pmatrix}^2\left.\frac{d\sigma}{d\Omega}\right|_{j_1'\kappa;j_10}. \quad (37)$$

When $j_1=j_1'=0$, these relations reduce to the IOS factorization relations already known in the atom–diatom case[45]; our demonstration is, however, less restrictive since it does not involve the centrifugal decoupling approximation.

F. Numerical calculations and results

The coupled equations (25) have been solved using the Fox–Goodwin method[47] with a basis of $j_1=0$, 2, and 48 Gauss–Legendre γ_2 values. The whole calculation of S matrices and differential cross sections takes 3 min of computation time on an IBM 370/168. Using Relation (37), we can generate the whole set of differential cross sections necessary to analyze the data.

We see on Fig. 5 the differential cross sections for single excitation (CO alone) and double excitation. The oscillatory structure is due to diffraction oscillations.

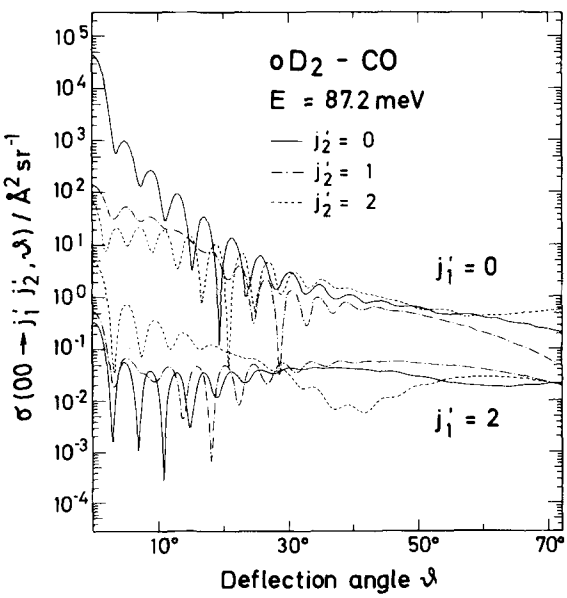

FIG. 5. Calculated differential cross sections for the rotational excitation of $D_2(j_1')$ and $CO(j_2')$ small angle scattering. The oscillations are mainly due to diffraction.

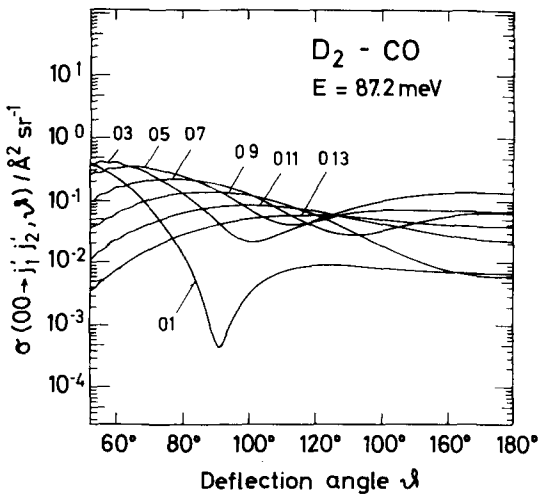

FIG. 6. Calculated differential cross sections for the rotational excitation of D_2 (first number) and CO (second number) starting from 00 for large angle scattering. The rotational rainbow maxima move towards large angles with increasing final j.

Double excitation cross sections are much smaller than single excitation cross sections which is due to the small D_2 anisotropy in the potential surface[20,21] and to the large rotational constant of D_2. It is interesting to note that the diffraction oscillations for the different transitions are partly out of phase, which explains the damping of this structure in the total differential cross section.

Figure 6 shows the large angle differential cross sections for CO excitation. Rotational rainbows peak at increasing ϑ values with increasing Δj.[13–18] The minimum in the $00\rightarrow 01$ cross section comes from nearly perfect cancellation in the attractive and repulsive parts of the $v_{010}(r)$ terms of the potential.

Figure 7 shows the effect of the initial rotational state of the CO molecule for CO rotational excitation cross sections at fixed deflection angle and variable final j_2'. The cross sections show two maxima as is expected for the rotational rainbow structure of a heteronuclear molecule (see the discussion in Sec. IV). Cross sections are larger for even Δj transitions at low Δj values but larger for odd Δj in the large Δj rotational rainbow region. This effect is due to interference between even and odd terms in the potential and has been already demonstrated by McCurdy and Miller[48] using semiclassical methods. The factorization relations (37) displace the peaks in $01\rightarrow 0j_2'$ compared to $00\rightarrow 0j_2'$. Thus, on cross sections averaged over the initial state distribution the structure is washed out.

IV. COMPARISON BETWEEN EXPERIMENT AND THEORY

A. Total differential cross sections

With the theoretical formalism developed in Sec. III we are now able to compare the experiments with calculations based on the potential surface of Ref. 21. First we compare the total differential cross sections. The

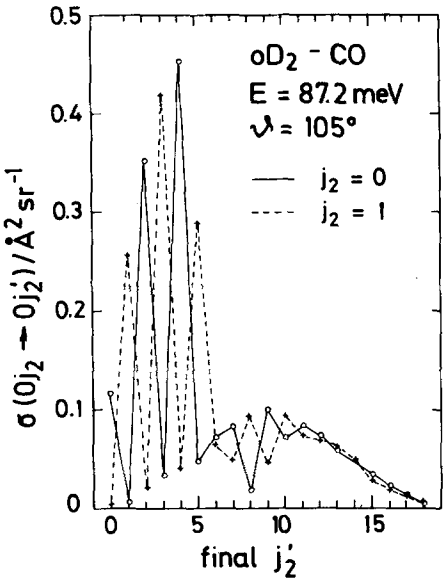

FIG. 7. Calculated cross sections for the rotational excitation of CO for a fixed angle and two different initial states. The two peaks and the interference oscillation within the first peak are due to rotational rainbow structure for heteronuclear molecules.

calculations have been performed as follows: The individual state-to-state differential cross sections are summed according to the initial state distribution (see Table I), averaged over the velocity and angular distribution, and transformed with the correct Jacobians and velocity corrections into the laboratory system. The final result is displayed in Fig. 1. The comparison does not look very satisfactory. There are two discrepancies to be observed. First, diffraction oscillations are out of phase with the calculated distance from peak to peak being too large. Second, the general falloff of the envelope of the oscillations is not steep enough for the calculation. It is generally assumed that the total differential cross section depends (at least in the small angle regime) mainly on the isotropic part of the potential since it is dominated by the elastic transitions (see Fig. 5). Therefore, the size parameters of the isotropic potential have to be changed as follows: The minimum distance which is given by the position of the diffraction oscillations according to[49]

$$R_m = \pi/(k \cdot \Delta\vartheta) \tag{38}$$

should become larger. The potential well depth ϵ can be estimated for the present case according to the Regge expansion by

$$\epsilon \sim \vartheta_R \sim (\mathrm{Im}\,\lambda_R)^{-1} , \tag{39}$$

where ϑ_R is the rainbow angle and $\mathrm{Im}\,\lambda_R$ is the imaginary part of the Regge pole, which dominates the falloff of the differential cross section $I(\vartheta) \simeq \exp(-2\vartheta\,\mathrm{Im}\,\lambda_R)$.[50-52] According to Eq. (39), ϵ should become smaller.

Since we would like to scale the measured time of flight distribution in an absolute way to the total differential cross section, we have tried to find a better isotropic potential which describes the small angular part

TABLE II. Potential parameters of V_0.

	Calculation	Experiments		
	Ref. 21	$Q(v)$, Ref. 23	$I(\vartheta)$, Ref. 22	$I(\vartheta)$, this work
ϵ (meV)	9.80	5.74	6.90±1.5	5.73±0.3
R_m (Å)	3.70	3.52	3.93±0.1	3.88±0.08

of the total differential cross section. As a potential model we have used the Hartree–Fock dispersion form[53-55] with a suitable cutoff function $f(r)$ for small r:

$$V_0(r) = A\exp(-\beta r) - (C_6 r^{-6} + C_8 r^{-8})\, f(r) , \tag{40}$$

with

$$f(r) = \begin{cases} \exp[-4(R_m/r - 1)^3] , & r \le R_m , \\ 1 , & r \ge R_m . \end{cases} \tag{41}$$

For convenience, we have replaced two parameters A and C_8 by ϵ and R_m using

$$\begin{aligned} A &= \exp(\beta R_m)\,[(8\epsilon - 2C_6 R_m^{-6})\,(\beta R_m - 8)^{-1}] , \\ C_8 &= R_m^8 (\beta R_m - 8)^{-1}\,[(C_6 R_m^{-6}(6 - \beta R_m) + \epsilon\beta R_m] . \end{aligned} \tag{42}$$

We have fixed the parameters $C_6 = 19.181$ eV Å^6 according to Ref. 56 and $\beta = 4.8354$ Å^{-1} according to Ref. 21, and fitted ϵ and R_m by comparison with the measured data. The final results for ϵ and R_m are given in Table II. For the related parameters, we get $A = 4.5197 \times 10^5$ eV and $C_8 = 170.68$ eV Å^8. The values for the asymptotic coefficients of the *ab initio* potential $C_6 = 22.1$ eV Å^6 and $C_8 = 107.7$ eV Å^6 deviate from the results of the fitted potential. The cross sections based on this V_0 potential and the anisotropy of the *ab initio* potential are also plotted in Fig. 1. Now the agreement is much better than for the pure *ab initio* potential. Table II also contains the potential parameters determined for the present system by two other molecular beam experiments.[22,23] The values of the present paper are generally, within the experimental errors, in agreement with the other experiments (if we take into account that in Ref. 23 only the product of ϵR_m is measured with a reasonable accuracy). However, the results deviate from the calculation starting from the *ab initio* potential. By means of the new potential parameters, we are able to scale the small angular part and thus the complete total differential cross section absolutely. The absolute values which result for those angles where time of flight distributions have also been measured are listed in Table III.

TABLE III. Absolute total differential cross sections.

Θ (lab)	ϑ (c.m.)	$I(\vartheta)$ (Å^2 sr^{-1})
30°	36°	4.68
40°	49°	3.30
50°	63°	2.49
60°	77°	2.09
70°	91°	1.71
80°	105°	1.50

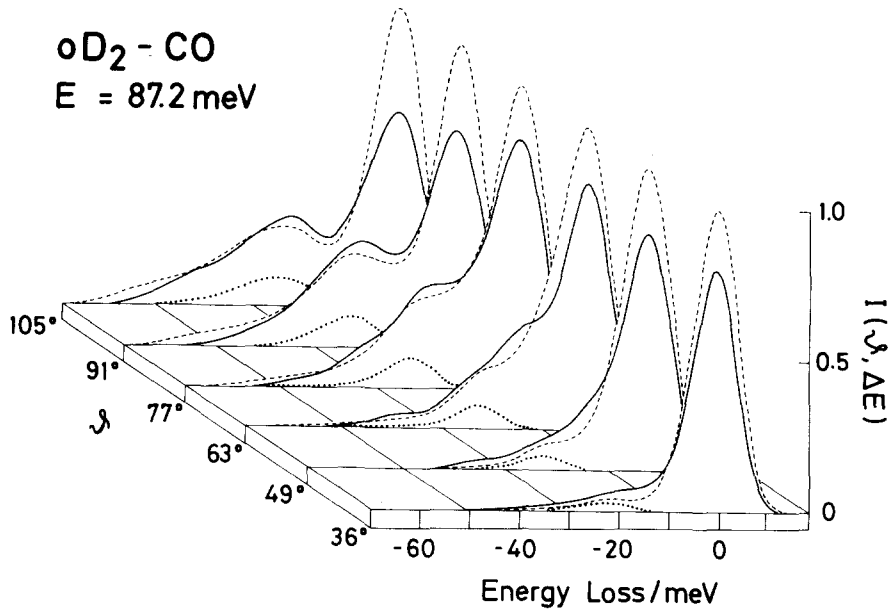

FIG. 8. Comparison of measured (solid line) and calculated (dashed line) energy loss spectra using the *ab initio* potential of Ref. 21. The dotted line marks the contribution due to the excitation of both molecules. The area of the peaks for each angle gives the differential cross section in absolute units (see Table III). The intensities I for different angles are arbitrarily normalized to the maximum of the calculated spectrum.

B. Double differential cross section

Now we are able to compare the area of the measured time of flight spectra which is given by the values of Table III with the calculations based on the potential of Ref. 21. We proceed as follows: First of all we calculate individual cross sections for all open channels starting from $j=0$ of D_2 and CO. The cross sections for the other two initial rotational states of CO $j=1$ and $j=2$ are generated using the factorization formula of Eq. (37). The cross sections are summed according to their initial states and the transferred energy ΔE_{if} [see Eq. (2)], and then convoluted as described by Eq. (5). The resulting distribution function can be directly compared to the measured values. This comparison is made in Fig. 8. Note that the comparison for each angle is absolute, but the values from angle to angle are arbitrarily normalized to the maximum of the calculated distribution. The striking feature of this comparison is that the essential characteristics of the measurements, a large peak at small values of j' and a smaller peak at larger values of j' and large scattering angles, are also present in the calculations. In addition, there is a nearly perfect agreement of the positions of the peaks. The second peak's smaller amplitude is also nearly reproduced if we take into account the experimental error. The only marked deviations occur for the amplitude of the first dominating peak which is too large in the calculation.

It is very interesting to examine the influence of different initial rotational state distributions on the final result. For the correct initial state distribution 0.51 ($j=0$), 0.43 ($j=1$), and 0.06 ($j=2$) and a drastic variation 0.25 ($j=0$), 0.40 ($j=1$), and 0.35 ($j=2$), we found nearly no change in the final result. The reason for this insensitivity is based on the fact that the amount of molecules in even or odd rotational states is about the same. The cross sections for all even or all odd initial values behave very similarly. However, they differ very much from each other, as can be seen from Fig. 7. Here, because of the nearly equal masses of C and O, the remnant of a selection rule where $\Delta j=2$ transitions are preferred can be seen at least for small j values. If we average an equal amount of even and odd states, the individual contributions are averaged out. We would only expect a completely different result for a nearly pure $j=0$ or $j=1$ initial state distribution.

The method of calculation allows us to distinguish between the excitation of the CO and the D_2 molecule, which is not possible by the present type of measurement. In Fig. 8 we use the dotted line to show the energy loss spectrum due to the excitation of *both* molecules. Comparing the ΔE's at which this double-molecule excitation occurs in Fig. 8 with the D_2 and CO rotational energy levels shown in Fig. 3, we can draw two conclusions. First, the larger peak is not affected by excitation of the D_2 due to the differences in rotational excitation threshold energies. Second, the double-molecule excitation is essentially all due to excitation of the D_2 molecule since the D_2 rotational excitation threshold in Fig. 3 coincides with the maximum in the double-excitation peak shown in Fig. 8. It is interesting to note that this contribution, though the individual cross sections are usually an order of magnitude lower than the cross sections for pure CO excitation (see Fig. 5), convoluted according to Eq. (5) is much larger, ranging from more than 50% at small angles where nearly no second peak is present to about 30% at large angles where the second peak is largest. The main reason for this behavior is the large number of accessible states, which all are summed by the present experimental method. On an absolute scale the D_2 contribution increases with increasing scattering angle as is expected for this type of weak anisotropic interaction.[30,31]

Thus, we can attribute the two peak structure, which is shifted to larger final angular momentum values with increasing deflection angle (see Fig. 4), to the excitation of the CO molecule. This structure resembles very much the rotational rainbow structure[13–18] which should give two peaks because of the heteronuclear char-

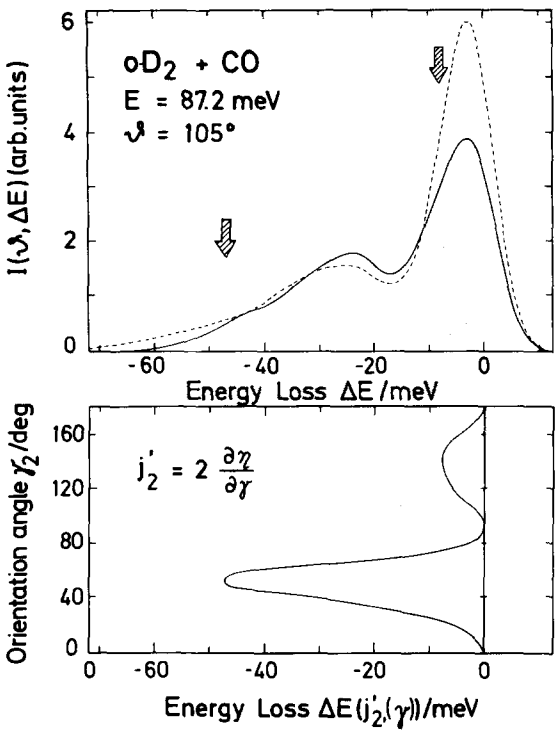

FIG. 9. Upper part: Measured energy loss spectrum (solid line) and calculation using the *ab initio* potential (dashed line) for $\vartheta = 105°$. The arrows mark the position of the classical rotational rainbow j'_R in the energy loss scale. Lower part: Excitation function (final rotational state) j' expressed by the energy loss ΔE as a function of the orientation angle of CO from the same calculation. $\gamma_2 = 0$ marks the C side and $\gamma_2 = 180°$ the O side of the molecule.

acter of CO.[13,15(b),17,57] To check this behavior more carefully we have performed a phase shift analysis since in the IOS approximation the final angular momentum is given by $j' = 2\partial\eta/\partial\gamma$. The result is illustrated in Fig. 9. In the upper graph we reproduce a measured and a calculated energy loss spectrum and indicate with the arrows the position of the (j'-dependent) classical rotational rainbow. Note that in Fig. 9 we show the j' dependence of various quantities through the dependence of those quantities upon the energy loss ΔE, which is itself a function of j'. In the lower part we give the dependence of the energy loss as a function of the CO/D_2 orientation angle γ_2, which is defined so that $\gamma_2 = 0°$ marks the C side and $\gamma_2 = 180°$ marks the O side. As is clearly seen, there are two extreme values of j' which are correlated with the maxima of the measured spectrum. Due to the semiclassical treatment, the maximum of the $j'(\gamma)$ curve corresponds to 44% of the measured peak intensity.[17] It should be noted that such a simple relationship is only valid if $\partial\theta/\partial J \cdot \partial j'/\partial\gamma \gg \partial\theta/\partial\gamma \cdot \partial j'/\partial J$ and if there is a one-to-one correspondence of the deflection angle and the total angular momentum (neglect of the normal rainbow structure). The interesting point of this result is that we can correlate particular deviations of calculations from measurements to particular features of the potential surface since certain j' values correspond to certain orientation angles γ_2 of the CO molecule with respect to the incoming D_2.

C. Discussion

Before we draw some conclusions about the ability of the potential surface to reproduce the present type of measurements, we have to discuss the approximations involved in the calculation of cross sections. The excitation of D_2 can be treated in the CS approximation without any problem.[30] The anisotropy is small and mainly occurs in the repulsive part of the potential. Thus, the centrifugal decoupling approximation is valid. As for the treatment of the CO excitation in the IOS approximation, we have to be a little more careful. Again we are only interested in an angular regime outside the diffraction oscillations, which means that only the repulsive part of the potential is probed and the decoupling of the orbital angular momentum is a good approximation. However, in addition, for the IOS approximation the molecular angular momentum j is also decoupled, which means that the energy transfer ΔE must be small compared to the collision energy. An inspection of Fig. 4 clearly indicates that the energy transfer of the first peak never exceeds 6% and that of the second peak is around 25% of the collision energy. Thus, the IOS approximation appears to be a reasonable approximation for this range. However, for the largest energy transfer measured in the tails of the distributions, the IOS approximation is no longer a good approximation. Thus, the deviations between measured and calculated cross sections in Fig. 8 for very large energy transfers are obviously due to a failure of the approximation and not due to the potential (the calculated intensity is as expected larger than the measurement). Since the IOS approximation does hold for small energy transfers, we are now able to discuss the reliability of the potential energy surface[21] at these small ΔE.

From the measurement of the small angle scattering of the total differential cross sections we are able to derive some information on the isotropic interaction potential around the minimum and the near repulsive part. The potential well depth has to be lowered appreciably, whereas the zero point should be slightly shifted to larger values (see Table II).

From the rotationally inelastic scattering we get some information on the anisotropy of the potential surface, mainly in the repulsive region from the minimum up to 70 meV. Calculations and measurements roughly agree for $\Delta E \geq 22$ meV where D_2 excitation is possible. Thus, we indirectly conclude that the anisotropy of the D_2 is correctly described by the surface. This is confirmed by the regular behavior of these cross sections (see Fig. 8). Therefore, we can concentrate on the anisotropy of the CO excitation averaged over the D_2 orientations. A simple two dimensional model based on a rigid ellipsoid shows that the final angular momentum is proportional to the wave number k, the $\sin\vartheta/2$, and parameters of the rigid ellipsoid. Since the positions of the rotational rainbow structure for both peaks agree with the calculation, we conclude that the general form of the anisotropy expressed by the difference of the two axes $R_a - R_b$ and the shift δ between center of mass and center of symmetry are correct. According to the model of Ref. 57, the axes are defined by $V(R_a, \gamma = \pi) = E$ and $V(R_b, \gamma = \pi/2) = E$, where E is the energy

which is probed at the different angles and which is, for example, for $\vartheta = 105°$ about $E = 70$ meV. As for the amplitudes of the two peaks, there is agreement for the larger j' values. According to Fig. 9, we conclude that the surface $V(R,\gamma)$ around $\gamma = 45°$ is correct; however, around $\gamma = 135°$, where D_2 approaches the O end of CO, the anisotropy has to be changed in order to account for the overestimation of the cross section. An inspection of the semiclassical analysis of the rotational rainbow structure indicates[15(b),17] that the amplitudes are essentially proportional to $|\partial j'/\partial\gamma|^{-1}$. Therefore, the curvature of $\eta(\gamma,J)$ with respect to γ, and thus roughly the curvature of the potential, has to be increased or the point of zero j' has to be shifted to the O side of the molecule. Since, on the other hand, the maximum of j' is fixed (agreement between calculation and experiment), j' and thus the anisotropy of the potential $\partial V/\partial\gamma$ have to be lowered. These results are in essential agreement with the findings from other sources. A recent study on the rotational relaxation of CO by collision with H_2[24] gives an overestimation of absolute cross sections by the theory, though it is believed that in contrast to the present study the experiments are more sensitive to the attractive part of the potential.

V. SUMMARY

In summary, the present study has demonstrated the usefulness of doubly differential cross sections with respect to angle and energy loss in probing the anisotropy of the potential surface. One of the essential conditions is to have a reliable method to transform the unresolved (with respect to single rotational transitions) spectra to the center of mass system so that not only positions but also amplitudes can be compared with calculation.

This comparison shows that the cross sections for the CO excitation are much larger than for the D_2 excitation. The energy loss spectra consist essentially of two rotational rainbow maxima. The maximum at large j' is due to a rotational rainbow originating from the CO excitation on the C side of the molecule; the maximum of low j' with larger probability is due to the excitation on the O side of the molecule. The comparison with calculations using the potential surface of Ref. 21 shows agreement for the positions and the amplitudes of the large j' maximum. However, the calculation overestimates the amplitudes of the low j' maximum. This suggests that the surface has to be changed near the O side of the molecule by increasing the curvature of the anisotropy or by a displacement of the point of zero rotational excitation towards the O side. It should be mentioned that these conclusions are based on the IOS approximation which might not be valid for large Δj transfers.

Note added in proof: G. H. Diercksen and W. P. Kraemer recently calculated the H_2–CO surface with an enlarged basis set. Their surface has indeed a smaller value for $\partial V/\partial\gamma$ in the region where the H_2 molecule approaches the O atom.

ACKNOWLEDGMENTS

We thank Dr. J. Schleusener for useful discussions on the evaluation of the data and Dr. G. Pfeffer for carefully reading the manuscript. The numerical calculations in Göttingen have been performed at the GWD, Göttingen.

[1]M. Faubel and J. P. Toennies, Adv. At. Mol. Phys. **13**, 229 (1977).
[2]H. Thuis, S. Stolte, and J. Reuss, Comments At. Mol. Phys. **13**, 229 (1977).
[3]R. B. Gerber, V. Buch, U. Buck, G. Maneke, and J. Schleusener, Phys. Rev. Lett. **44**, 1397 (1980).
[4]H. Schmidt, V. Hermann, and F. Linder, J. Chem. Phys. **69**, 2734 (1978).
[5]M. Faubel and J. P. Toennies, J. Chem. Phys. **71**, 3770 (1979).
[6](a) U. Buck, F. Huisken, and J. Schleusener, J. Chem. Phys. **68**, 5654 (1978); (b) U. Buck, F. Huisken, J. Schleusener, and J. Schäfer, *ibid.* **72**, 1512 (1980).
[7]W. R. Gentry and C. F. Giese, J. Chem. Phys. **67**, 5389; W. R. Gentry and C. F. Giese, Phys. Rev. Lett. **39**, 1259 (1977).
[8]M. Faubel, K. H. Kohl, and J. P. Toennies, J. Chem. Phys. **73**, 2506 (1980).
[9]P. J. Dagdigian, B. E. Wilcomb, and M. A. Alexander, J. Chem. Phys. **71**, 1670 (1979).
[10]K. Bergmann, R. Engelhardt, U. Hefter, and J. Witt, J. Chem. Phys. **71**, 2726 (1979); U. Hefter, P. L. Jones, A. Mattheus, J. Witt, K. Bergmann, and R. Schinke, Phys. Rev. Lett. **46**, 915 (1981).
[11]J. A. Serri, A. Morales, W. Moskowitz, D. E. Pritchard, C. H. Becker, and J. L. Kinsey, J. Chem. Phys. **72**, 6304 (1980).
[12]W. Eastes, U. Ross, and J. P. Toennies, Chem. Phys. **39**, 407 (1979).
[13](a) W. Schepper, U. Ross, and D. Beck, Z. Phys. A **290**, 131 (1979); (b) D. Beck, U. Ross, and W. Schepper, Phys. Rev. A **19**, 2173 (1979).
[14]L. D. Thomas, J. Chem. Phys. **67**, 5224 (1977).
[15](a) R. Schinke, Chem. Phys. **34**, 65 (1977); (b) R. Schinke, J. Chem. Phys. **71**, 1120 (1980); (c) **73**, 6117 (1980).
[16]J. M. Bowman, Chem. Phys. Lett. **62**, 309 (1979).
[17]J. Korsch and R. Schinke, J. Chem. Phys. **73**, 1222 (1980).
[18]S. Bosanac, Phys. Rev. A **22**, 2617 (1980).
[19]H. Pauly in *Atom–Molecule Collisions*, edited by R. B. Bernstein (Plenum, New York, 1979).
[20]J. Prissette, E. Kochanski, and D. R. Flower, Chem. Phys. **27**, 373 (1978).
[21]D. R. Flower, J. M. Launay, E. Kochanski, and J. Prissette, Chem. Phys. **37**, 355 (1979).
[22]A. Kuppermann, R. J. Gordon, and M. J. Coggiola, Discuss. Faraday Soc. **55**, 145 (1973).
[23]H. P. Butz, R. Feltgen, H. Pauly, and H. Vehmeyer, Z. Phys. **247**, 70 (1971).
[24]Ph. Brechignac, A. Picard-Bersellini, R. Charneau, and J. M. Launay, Chem. Phys. **53**, 165 (1980).
[25]See D. J. Kouri, in *Atom–Molecule Collisions*, edited by R. B. Bernstein (Plenum, New York, 1979).
[26]P. McGuire and D. J. Kouri, J. Chem. Phys. **60**, 2488 (1974); R. T Pack, *ibid.* **60**, 633 (1974).
[27]D. M. Chase, Phys. Rev. **104**, 838 (1956).
[28]P. G. Burke, Adv. At. Mol. Phys. **15**, 741 (1978).
[29]T. P. Tsien and R. T Pack, Chem. Phys. Lett. **6**, 54 (1970).
[30]J. Andres, U. Buck, F. Huisken, J. Schleusener, and F. Torello, J. Chem. Phys. **73**, 5620 (1980).
[31]U. Buck, F. Huisken, J. Schleusener, and J. Schäfer, J. Chem. Phys. **74**, 535 (1981).
[32]D. Bassi, A. Boschetti, S. Marchetti, G. Scoles, and M. Zen, J. Chem. Phys. **74**, 2221 (1981).
[33]A. Kohlhase, Diplomarbeit, Universität Göttingen, 1981.
[34]R. B. Gerber, M. Shapiro, U. Buck, and J. Schleusener, Phys. Rev. Lett. **41**, 236 (1978); R. A. Aziz, P. W. Riley,

U. Buck, G. Maneke, J. Schleusener, G. Scoles, and U. Valbusa, J. Chem. Phys. 71, 2637 (1979).
[35]H. Meyer, Diplomarbeit, Universität Göttingen, 1981.
[36]See M. Shapiro, R. B. Gerber, U. Buck, and J. Schleusener, J. Chem. Phys. 67, 3570 (1977).
[37]I. Shimamura, Chem. Phys. Lett. 73, 328 (1980).
[38]J. M. Launay, J. Phys. B 9, 1823 (1976).
[39]M. Jacob, G. C. Wick, Ann. Phys. (N.Y.) 7, 404 (1959).
[40]H. Klar, Z. Phys. 228, 59 (1969); H. Klar, Nuovo Cimento Soc. Ital. Fis. A 4, 529 (1971).
[41]H. E. Moses, Ann. Phys. (N.Y.) 60, 275 (1970).
[42]M. E. Rose, *Elementary Theory of Angular Momentum* (Wiley, New York, 1957).
[43]A. Messiah, *Mecanique Quantique* (Dunod, Paris, 1964), Vols. I–II.
[44]J. M. Launay, J. Phys. B 10, 3665 (1977).
[45]R. Goldflam, S. Green, and D. J. Kouri, J. Chem. Phys. 67, 4149 (1977); R. Goldflam, D. J. Kouri, and S. Green, *ibid.* 67, 5661 (1977); R. Schinke and P. McGuire, Chem. Phys. 31, 391 (1978); G. A. Parker and R. T Pack, J. Chem. Phys. 68, 1585 (1978); V. Khare, *ibid.* 68, 4631 (1978).
[46]J. M. Launay, Chem. Phys. Lett. 72, 152 (1980).
[47]D. W. Norcross and M. J. Seaton, J. Phys. B 6, 614 (1973).
[48]C. W. McCurdy and W. H. Miller, J. Chem. Phys. 67, 363 (1977).
[49]U. Buck, Adv. Chem. Phys. 30, 313 (1975).
[50]K. W. McVoy, Lecture Notes Phys. 33, 127 (1975).
[51]J. N. L. Connor and W. Jackubetz, Mol. Phys. 35, 949 (1978).
[52]S. Bosanac, R. B. Gerber, and U. Buck, Chem. Phys. Lett. 58, 359 (1978).
[53]R. Ahlrichs, P. Penco, and G. Scoles, Chem. Phys. 19, 119 (1977).
[54]K. T. Tang and J. P. Toennies, J. Chem. Phys. 68, 5501 (1978).
[55]R. J. LeRoy and J. S. Carley, Adv. Chem. Phys. 42, 353 (1980).
[56]G. A. Parker and R. T Pack, J. Chem. Phys. 64, 2010 (1976).
[57]S. Bosanac and U. Buck, Chem. Phys. Lett. 81, 315 (1981).